Arc fault power balance in AC and DC electrical aeronautic networks: influence of pressure and cable material

T Vazquez, P Teulet, F Valensi, A Risacher, M Masquère

Arc fault power balance in AC and DC electrical aeronautic networks: influence of pressure and cable material

T Vazquez[1,2], P Teulet[2], F Valensi[2], A Risacher[1] and M Masquère[2]

[1]IRT Saint-Exupery, B 612, 3 rue Tarfaya, CS 34436, 31405 Toulouse cedex 4, France

[2]Université de Toulouse, UPS, INPT, LAPLACE (Laboratoire Plasma et Conversion d'Energie), 118, route de Narbonne, 31062 Toulouse cedex 9, France

E-mail: thomas.vazquez@irt-saintexupery.com

Abstract. A systematic study of arc faulting between two cables in aeronautic conditions is performed and a power balance of the arc is realised. Electrical characteristics and radiative heat flux are recorded. The effect of the current mode (AC/DC), cable material and pressure are highlighted with the assessment of the power balance, that includes the mean power of the arc, the power transferred to the cables that can cause melting and vaporisation, and the power lost by radiation, conduction and convection in the arc column. The evaporated mass of the cables can be estimated in this way. Optical Emission Spectroscopy (OES) measurements of the induced plasma are performed rendering the overall temperature of the arc using a Boltzmann plot method. The overall temperature is higher for copper contaminated plasma than for aluminium contaminated plasma. Despite the erratic behaviour of the plasma, the trend shows the DC current as well as the use of lighter aluminium based cables lead to a higher power.

Keywords: Electric arc, aeronautic cable, thermal plasma, arc fault, arc tracking

1. Introduction

Arc faults occurring in wiring systems, also called "arc tracking phenomenon", are an issue known for decades in the aeronautic industry [1, 2] and space application [3–5]. With a significant amount of energy released in a very short time, arc faults can severely damage electrical installations and lead to dramatic accidents. In the past, the use of passive protection (appropriate insulating materials and segregation distances) as well as active protection devices (Arc Fault Circuit Interrupters) gave good results to avoid the ignition of an arc, or at least limit its damages. However, changes to come for the next generation of aircraft with new electrical systems design, imply to assess and/or renew safety measures against arcing. These changes come with the concept of a More Electric Aircraft (MEA) [6]. The replacement of pneumatic and hydraulics systems by their electrical counterparts (for weight reduction and hence, fuel consumption concerns) as well as a rising demand for comfort devices, result in an increase of the electrical power embedded in the next generations of aircrafts [7]. This electric power is deployed in the aircraft through the cables, which are in return, an important parameter regarding the weight of an aircraft (for example, there is around 530 km of total cable length in an A380). There are at least three ways to deploy more power in these cables and to obtain a weight reduction. First and foremost, instead of using higher current levels, which would increase the section of the wires and thus their weight, the use of higher voltages is foreseen (the first step is the use 540 Vdc, then it is expected to reach voltages up to 3 kV). Second, electric distribution changes from AC to DC systems. This could reduce the number of cables, since AC architectures are three-phase while only two cables are needed in DC [8]. Finally, for weight reduction concerns, the use of aluminium cables tends to replace copper cables. All of these changes can affect the propagation, the behaviour and consequently, the damages due to an arc fault. Most studies about arc faults are related to circuit breakers, switching devices, lightning, or arc welding [9–14, 17, 18, 29]. In the present study, arc faults between cables are investigated in order to quantify the effects on their environment.

The aim of this work is to establish a power balance of the arc, , and to highlight the effect of the current mode (AC/DC), the cable material and the pressure. In order to be in agreement with the concerns of aircraft designers, the current and the cables section are set as constant parameters. In the case of a constant impedance, the power should be the same in DC than in AC for the same RMS current value. However, for an electric arc in AC, when the voltage becomes lower than the value needed to sustain the arc, extinction occurs and current (thus power) drops to zero. This results in a higher power in the case of DC than for AC. This work aims to quantify this difference, since more power in DC could induce more damages. This comparison is made for copper (Cu) and aluminum (Al) cables for two pressure values, at ground level (100 kPa) and at certification altitude (9.5 kPa). For both cases, the mean power of the arc, the power transferred to the cables that causes melting and vaporising, and the power lost by radiation, convection and

conduction in the arc column is evaluated. Plasma temperature is an important parameter to characterise the arc, in particular concerning the estimation of the radiated losses in the power balance. However, it is difficult to get such information because of the very erratic behaviour of the arc fault, dominated by electrodes ablation. In previous works [15, 16], we used values from literature for comparable configuration. In this study we made a first attempt to experimentally measure the plasma temperature through Optical Emission Spectroscopy (OES) measurements. The spatially-resolved temperature could not be obtained because of the unpredictable pathway of the arc. The resulting overall plasma temperature is obtained using the Boltzmann plot method applied to emission lines of copper. The Boltzmann plot method is widely used in thermal and non-thermal plasmas (see for example [17, 18, 20–24]), but to the best of our knowledge, there are no published studies reporting the use of this method on arc faults between cables. Due to non reproducible nature of the arc, only statistical trends are deduced over numerous arc fault tests.

The section 2 describes the experimental set up used in this work. The methodology employed to achieve the power balance of the arc is explained in the section 3. The obtained results are presented in the section 4, and finally, a conclusion is given in section 5. .

2. Experimental setup

2.1. Test conditions

Figure 1 shows the experimental set up used for our study. The arc faults are generated between two aeronautic cables. This is a parallel arc configuration since each cable is connected to either + or - polarities in DC or phase 1 or 2 in AC. The voltage between the two electrodes (open circuit) is set to 400 V RMS at 800 Hz in AC and 400 V in DC. In air, the product of the distance d between the two electrodes (around 2 mm) and the the pressure p is too large to reach the breakdown voltage. This is why we need to bring down a droplet of salted water to trigger the arc. In order to facilitate arc ignition, a small part of the insulating material is removed (1 cm long and about 1/3 of the circumference of the cable, see figure 2). Cables are weighted before and after every experiment. By doing so, we obtain the ablated mass due to the erosion of the cables.

The current is set to 80 A in DC and 80 A RMS in AC, and the arc duration desired is 500 ms. Two pressure values are investigated: atmospheric pressure and 95 mbar. This latter value is a certification pressure, corresponding to a maximum altitude of approximately 15000 m, while a typical cruise altitude is about 10000-12000 m. Test conditions are summarised in table 1.

2.2. Material and measurements

We use the same power supply for every experiments (manufactured by Puissance Plus). It is capable of generating AC and DC wave forms up to 700 V at 124 A in DC and 400 V RMS at 350 A in AC. A schematic representation of the experimental set-up is given in figure 1. All

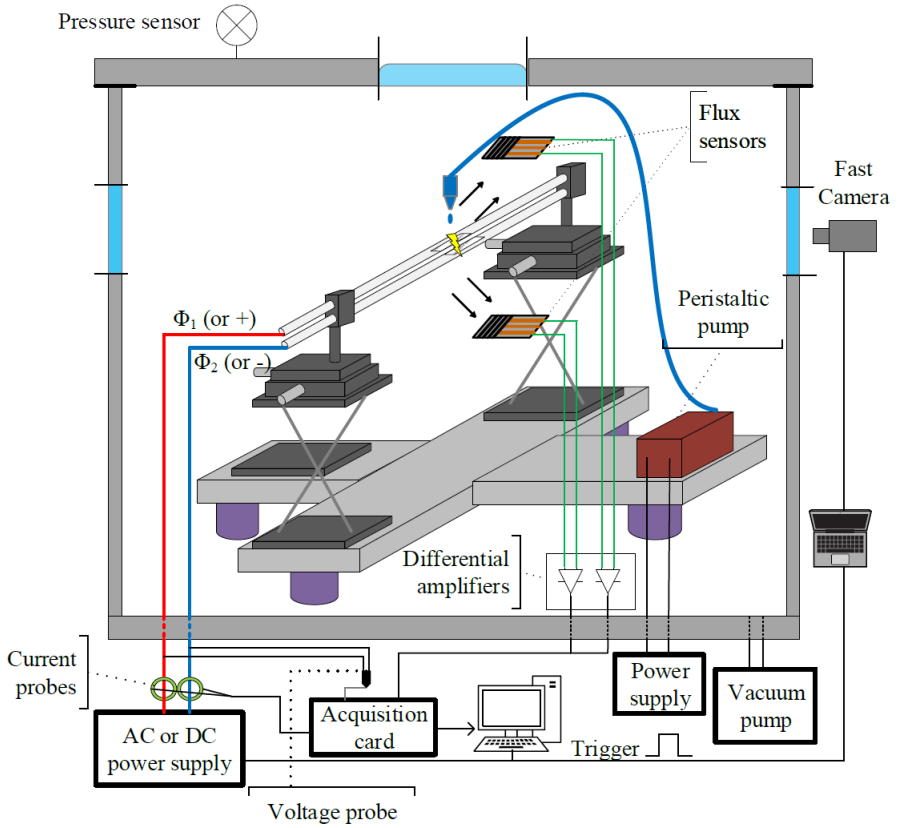

Figure 1: Scheme of the experimental set-up.

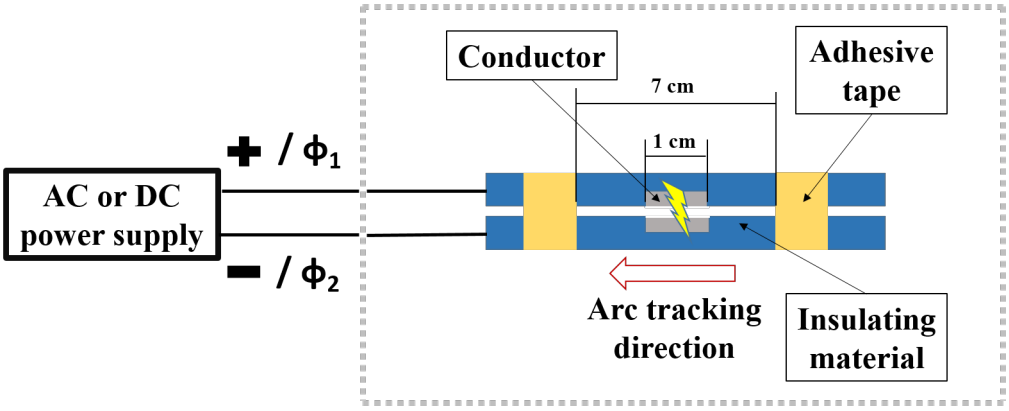

Figure 2: Schematic drawing of the cables.

	AC	DC
Open circuit voltage	400 V RMS at 800 Hz	400 Vdc
Arc current	80 A RMS	80 A
Maximum arc duration	500 ms	500 ms
Pressure	Atmospheric and 95 mbar	Atmospheric and 95 mbar

Table 1: Test conditions for copper and aluminium cables.

experiments take place in a 270 l chamber, allowing controlled pressure to reproduce ground or in flight operation. We place, inside this chamber, a peristaltic pump which is connected to an external power supply to drop the salted water.

The arc current is measured with Hall effect sensors (LEM LF 505-S), and the arc voltage with a differential voltage probe (Pintek DP-25) placed on each cable. Two radiative heat flux sensors are placed 9.5 cm away from the cables, facing the arc. They are radiative sensors based on thermocouples measuring all radiation included between 200 nm and 12000 nm, and they provide a voltage proportional to the radiative heat flux received from the arc. A high-speed camera (Phantom V9.1) is also used to record images of the arc at a frame rate ranging between 3 000 and 26 000 frames per second. All measurements are synchronised and recorded with the help of an acquisition board.

For each configuration mentioned above, aluminium and copper aeronautic cables are tested with the same gauge and same insulating materials. Their characteristics are presented in the table 2. Copper and aluminium cables have a different nominal current. At identical cable section, aluminium cables have a lower working current compared to copper. It is because aluminium is less conductive than copper, and current levels over the nominal one would heat the cable and age the insulating material prematurely.

	Copper cables	Aluminium cables
Conductor	Copper	Aluminium
Insulating materials	2 layers (polyimide + PTFE)	2 layers (polyimide + PTFE)
AWG (American Wire Gauge)	14	14
Nominal current	20 A	15 A

Table 2: Characteristics of the copper and aluminium cables used for arcing.

The electrical insulation is the same for both cables and is composed of two layers, see figure 3. The first layer, which is directly in contact with the conductor, is a polyimide layer (Kapton), and the second one is a PTFE layer (Teflon).

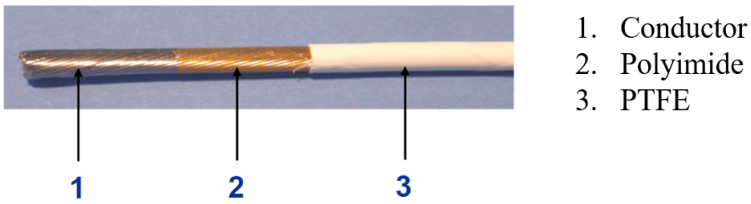

Figure 3: Composition of the aluminium and copper cables used in this work.

Finally, we probed the plasma with Optical Emission Spectroscopy (OES) measurements. For OES measurements, the arcs were ignited with a DC power supply, 640 V open circuit voltage and current levels ranging from 10 A to 100 A. Since the plasma is very erratic, we could not obtain any spatially-resolved spectra. Thus, instead of fixing the OES measurements in a single point, a collimator lens placed outside the chamber was used to collect all the light coming from the arc. The obtained results are therefore spatially integrated. The light passes through a wideband optical fiber cable to the spectrograph (Princeton Instruments Acton SpectraPro SP-2750) coupled with an EMCCD camera (Princeton Instruments ProEM-HS 1024BX3). Assuming that the plasma is in Local Thermodynamic Equilibrium (LTE), we used the Boltzmann plot method to obtain the overall plasma temperature. This method is well described in [17, 18, 21, 23] and the LTE assumption has been validated for many different types of arcs such as free-burning arcs [18] or arc welding [17, 18, 22]. Therefore, we apply this method by using the well-known atomic Cu I lines at 510, 515 and 521 nm [25]. These atomic Cu I lines were used for both copper and aluminium cables. For the

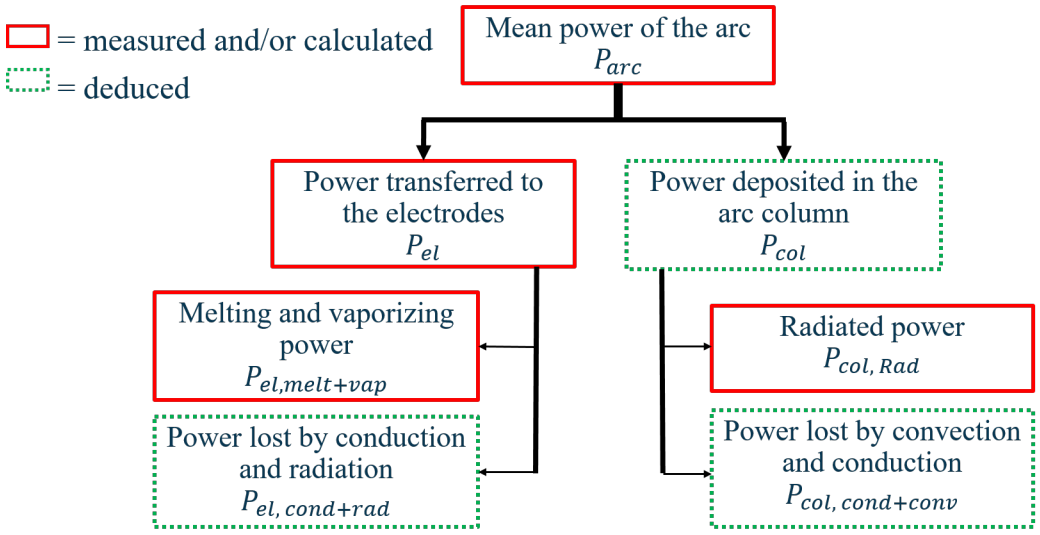

Figure 4: Power balance of the arc.

aluminium cables, the presence of a thin outer copper cladding on the inner aluminium core, allowed us to use the Cu I lines for the temperature determination. As the light collected by the collimator lens is coming from the whole arc, the resulting temperature represents a spatially-average value.

3. Power balance

We describe in this section, all the contributions to the power balance represented in figure 4.

To evaluate the different components of the power balance, we proceed as follows. We first calculate the mean electrical power (P_{arc}) that is provided by the power supply to the arc. Then, the mean power of the arc (P_{arc}) is divided in two components: the power deposited in the plasma column (P_{col}), and the power transferred to the electrodes (P_{el}). Each one is then split. The power in the arc column is lost by radiation ($P_{col,\,rad}$), conduction and convection ($P_{col,\,cond+conv}$). The power transferred in the electrodes melts and vaporises the cables ($P_{el,\,melt+vap}$). A small part of power is lost by radiation and conduction into the cables ($P_{el,\,cond+rad}$).

Some of the components are not directly obtained. Components in red rectangles in figure 4 are measured or calculated and those in green rectangles are deducted from the others. We now give a detailed description of the method used for the assessement of the power balance.

3.1. Mean power of the arc

The mean power of the arc is the total electrical energy divided by arc duration:

$$P_{arc} = \frac{E_{tot}}{t_{arc}} \tag{1}$$

with $E_{tot} = \int u(t) \times i(t)\, dt$ and t_{arc} is the arc duration.

We could not make an energy balance since the arc duration does not always reach the 500 ms. In some cases, arcs self extinguish before 500 ms. In order to make the comparison between every configurations, the energy is divided by the effective arc duration. Every power components are therefore a mean value over the arc duration.

Then, the total arc voltage is split in two parts [26], that is to say:

$$U_{arc} = U_{col} + U_{el} \tag{2}$$

where U_{el} is the sum of voltages drop at the cathode and the anode, and U_{col} is the voltage of the plasma column. By doing this, one can calculate the power transferred to the cables (see below, section 3.2) and deduct the power in the arc column (see 3.3).

3.2. Power transferred to the cables

As we did for the mean power, the power transferred to the electrodes is calculated likewise:

$$P_{el} = \frac{E_{el}}{t_{arc}} \tag{3}$$

with $E_{el} = \int U_{el} \times i(t)\, dt$

Where U_{el} is the total voltage drop at the electrodes ($U_{el} = V_A + V_C$). E_{el} is therefore the total amount of energy transferred to the electrodes. Based on prior studies [15, 16], we choose $U_{el} = 18\,V$ for copper electrodes and 19 V for aluminium at atmospheric pressure. For low pressure, $U_{el} = 12\,V$ was found for both cables [19]. The uncertainty on this value is $\pm\,2\,V$.

The power transferred to the electrodes causes the cable fusion and vaporisation and a small portion is lost by radiation and heat conduction into the cable. This is why this component is split as follows:

$$\begin{aligned} P_{el} &= P_{el,melt} + P_{el,vap} \\ &\quad + P_{insulation} + P_{el,cond+ray} \end{aligned} \tag{4}$$

The terms in equation (4) are discussed in the next sections.

3.2.1. Power spent for melting and vaporising of the cables

A significant part of the power generates the melting of the cables. This melting power is calculated using the weight loss of the electrodes, and is obtained with the relation:

$$\begin{aligned} P_{el,melt} &= \frac{1}{t_{arc}} \left(m_{melt} \times L_{melt} + Q_{melt} \right) \\ &= \frac{m_{melt}}{t_{arc}} \left(L_{melt} + \int_{T_{init}}^{T_{melt}} C_{sol}(T)\, dT \right) \\ &= \frac{m_{melt}}{t_{arc}} \times E_{melt} \end{aligned} \tag{5}$$

Where L_{melt} is the specific latent heat of fusion ($J.g^{-1}$), $Q_{melt} = m_{melt} \int_{T_{init}}^{T_{melt}} C_{sol}(T)\, dT$ is the heat transfer to get from room temperature (T_{init}) to the melting point (T_{melt}), C_{sol} is the specific heat capacity of the solid metal in $J.g^{-1}.K^{-1}$ [28] and m_{melt} is the ablated mass of metal in g.

Likewise, the calculation of the power spent for vaporising the electrodes is given by:

$$\begin{aligned} P_{elect,vap} &= \frac{1}{t_{arc}} \left(m_{vap} \times L_{vap} + Q_{vap} \right) \\ &= \frac{m_{vap}}{t_{arc}} \left(L_{vap} + C_{liq}(T_{vap} - T_{melt}) \right) \\ &= \frac{m_{vap}}{t_{arc}} \times E_{vap} \end{aligned} \tag{6}$$

Where L_{vap} is the specific latent heat of fusion ($J.g^{-1}$), $Q_{vap} = m_{vap}\, C_{liq}(T_{vap} - T_{melt})$ is the heat transfer to rise the temperature from the melting point (T_{melt}) to the boiling point (T_{vap}), C_{liq} is the specific heat capacity of the liquid metal in $J.g^{-1}.K^{-1}$ and m_{vap} is the vaporised mass of metal in g. The numerical values of E_{melt} and E_{vap} are given in table 3. m_{melt} is obtained through the weight loss method. We weigh the cables before and after each test. The loss of mass we measure is the ablated mass $m_{ablated}$ which includes the metal and a small part of insulation material. Knowing the mass distribution between metal and insulation material for a cable, both contributions of the ablated mass (metal and insulation material) can be obtained: $m_{ablated} = m_{melt} + m_{insulation}$, where $m_{melt} = \alpha \times m_{ablated}$ and $m_{insulation} = \beta \times m_{ablated}$, with α and β are the mass proportion of aluminium and insulation of the cable respectively. Here we assume that all ejected metal has been melted (confirmed with the high-speed imaging because the metal is ejected as droplet involving a fusion).

Then, the power corresponding to the ablation of the insulating material is given by:

$$P_{insulation} = \frac{m_{insulation}}{t_{arc}} \times E_{insulation} \tag{7}$$

taking $E_{insulation} = 2600\, J.g^{-1}$ from [27].

It is worth mentioning that the melted metal which may remain on the cables is taken into account for the weighing of m_{melt}.

	Copper	Aluminium
Density (g/cm^3)	8.96	2.70
Amount of substance (g/mol)	63.5	27
Melting point (K)	1358	933
Boiling point (K)	2843	2791
Melting energy E_{melt} (J/g)	672	1067
Vaporisation energy E_{vap} (J/g)	5493	13061
Total energy (J/g)	6165	14127

Table 3: Cu and Al properties. The energies of melting and vaporisation are calculated with data from [28].

The vaporised mass is much more difficult to obtain since we can not measure it directly. We know that it is a part of the melted mass ($m_{vap} = \gamma \times m_{melt}$) because the metal is first melted then vaporised. γ represents the fraction of vaporised metal. This value can be set either according to the literature (arbitrary between 1 and 10% of the melted mass), or, by using the power balance. In the latter case, the power balance lead us to find an upper bound of the vaporised mass of metal.. Indeed, we have $P_{el} = P_{el,melt} + P_{el,vap} + P_{insulation} + P_{el,cond+ray}$ where two unknowns left: m_{vap} and $P_{el,cond+ray}$. To avoid setting an arbitrary value of m_{vap}, we chose to make an assumption on $P_{el,cond+ray}$. The power lost by conduction in the cables and lost by electrodes' radiation is assumed to be negligible. It is clearly established from previous work that the power radiated from materials is negligible in the balance of energy exchanges at the electrodes [29–31].

Neglecting the power lost by conduction in the cable is less evident. However, since the power density is very high and localised on anode and cathode spots, high ablation rates of the cables occur and lead to the cooling of the electrode. With high current intensity levels, the vaporisation rate increases, and the losses by conduction in the electrode become negligible [32]. Therefore, we suppose that heat does not propagate deep inside the cable and it is mostly used to melt and vaporise the electrodes.

Considering these assumptions, the power lost by conduction in the cables and by radiation of the electrodes' surface is neglected:

$$P_{el,cond+ray} \simeq 0 \tag{8}$$

By neglecting this part of the power, we are now able to find an upper bound of the vaporised mass of metal. Results are given in section 4.

3.2.2. Power lost by conduction and radiation

As mentioned above, the power lost by conduction in the electrodes and by radiation of the electrodes' surface is considered as negligible.

3.3. Power dissipated in the arc column

Power dissipated in the arc column is deduced from the mean power and the power transferred to the electrodes as follows:

$$P_{col} = P_{tot} - P_{el} \tag{9}$$

The power dissipated in the arc column is split between the radiative losses (P_{rad}), that is measured (section 3.3.1), and the power lost by conduction and convection ($P_{col,cond+conv}$) deduced from the power balance (see section 3.3.2 below).

3.3.1. Power lost by radiation

In order to obtain the mean radiated power of the arc, a first step is to calculate the mean radiated heat flux received by the sensors:

$$\varphi_{moy} = \frac{1}{t_{arc}} \int_0^{t_{arc}} \varphi_{mes}(t)\, dt \tag{10}$$

where $\varphi_{mes}(t)$ is the time dependant measured heat flux in $W.m^{-2}$ and t_{arc} is the arc duration in s.

Assuming that the sensors are far enough and the arc is small, the arc is considered as a punctual source of light. Therefore, one can calculate the mean power radiated by the arc by integrating over a sphere:

$$P_{rad} = \int \varphi_{moy}\, dS = 4\pi l^2\, \varphi_{moy} \tag{11}$$

where l is the distance between the arc and the sensors. In some cases, the radiation emitted from the arc can be hidden by the cable. That is why we should place two of these sensors on different angle positions. Nevertheless, the radiated power is underestimated for at least two reasons. The first one is the absorption of the VUV radiation (< 200 nm) in the air on a very short distance and the second one is the presence of a lot of metallic vapour around the arc that possibly absorbs a part of the radiation.

3.3.2. Power lost by conduction and convection

This last component of the power balance is deduced from the power dissipated in the arc column and the power radiated by the arc column, and convection and conduction are grouped into one component:

$$P_{col,cond+conv} = P_{col} - P_{col,rad} \tag{12}$$

4. Results and discussion

In the section 4.1, we describe the behaviour of the arc fault with the help of the electrical characteristics and high-speed imaging. Section 4.2 gives the values of the ablated mass, electrode vaporisation and the specific erosion rate. These results are correlated with the section 4.3, which develop the obtained results of the power balance. Finally, a determination of the plasma temperature is given in section 4.5. It is noteworthy to mention that all results are given with a standard deviation, which is obtained by performing 5 arcs in the same conditions. For this study, standard deviations are quite important due to the erratic behaviour of the arc. Despite of a low reproducibility arc, we are able to find out trends and to highlight the effect of the parameters on the arc behaviour. Finally, we should mention that we could not perform arcs in alternative current at atmospheric pressure for copper cables. In these conditions, we observe that the arcs can not last longer than a few periods, due to the effect of null current step at every half period and the fact that copper cables can be more easily welded together during the default, leading to arc extinction.

4.1. Signals

Figures 5 and 6 show the typical signals of an AC and DC arc respectively. For both figures, arc voltages are in black and arc currents are in grey and the entire 500 ms arc duration are shown. For AC, we also show in a box, the beginning of the arc with a smaller time scale. Either in AC or DC, we can see the open circuit voltage (400 V in DC and 565 V peak in AC) just before arc ignition (t_0). Voltage drop takes place when the droplet of water falls on the cables. Then, the current goes up quickly to the desired value and is quite stable on average during the whole arc duration. It is not the case of the voltage which is increasing until the end. This is due to the ablation of the cables, inducing a longer arc column and therefore a higher arc voltage. Some current and voltage peaks may appear (mostly in DC). They appear because of growing instabilities in the arc. Arc column is expanding during very short times. We observe this phenomenon with the high speed camera, and a typical example is given in figure 7. For this example, the arc is realised with a DC power supply, 540 V open circuit voltage and a current intensity of 30 A. The arc is ignited between copper cables at atmospheric pressure. The camera is a Photron FastCam SA4 that recorded at 10 000 frames per second with an exposure time of 100 μs. The arc is first confined between the two cables (figure 7a) and 4 ms later, it suddenly expands widely (figure 7b).

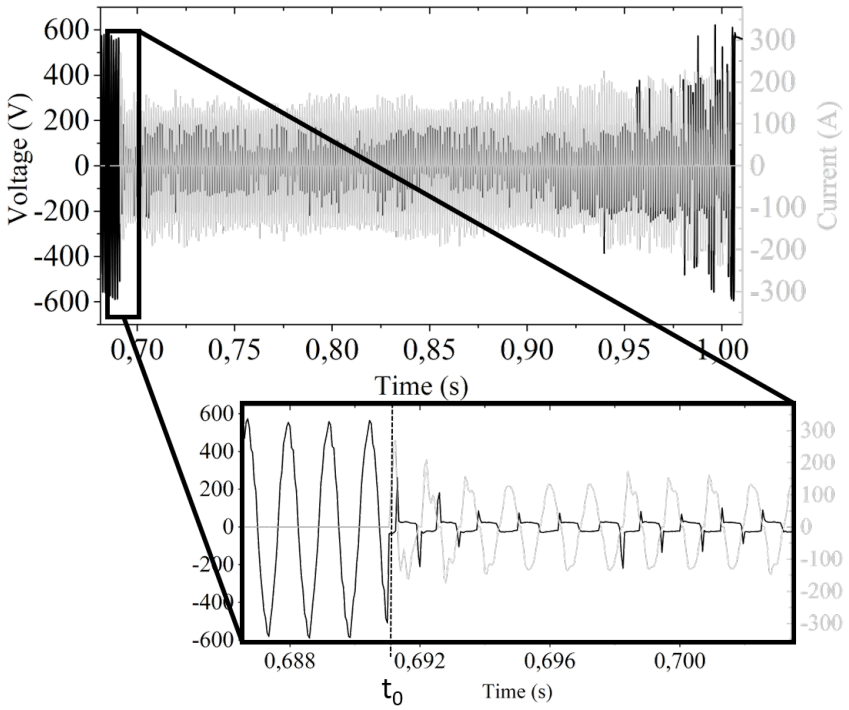

Figure 5: Typical arc current and voltage in AC.

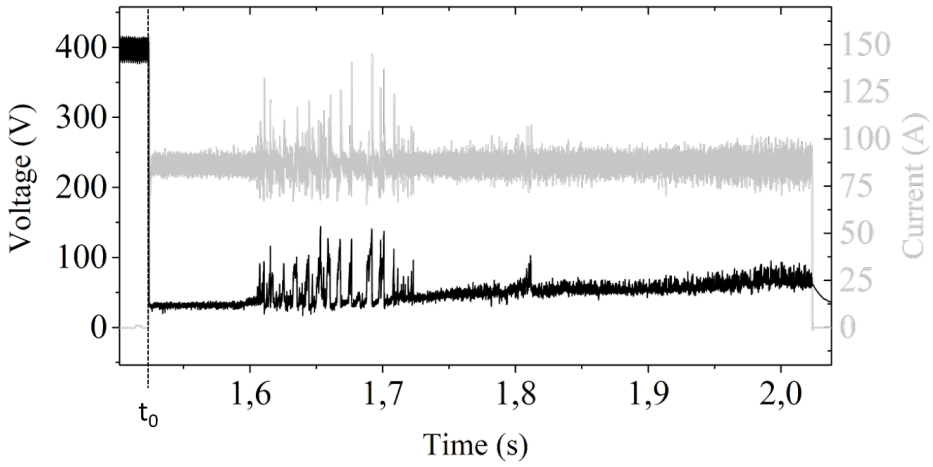

Figure 6: Typical arc current and voltage in DC.

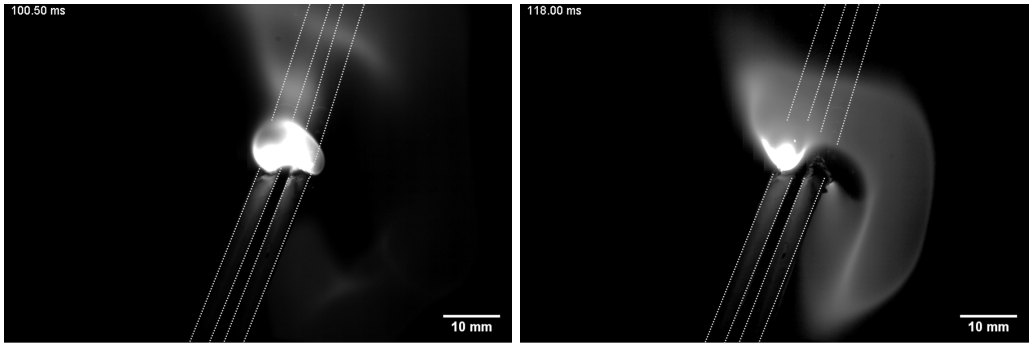

(a) t + 160.08 ms after arc ignition (b) t + 164.35 ms after arc ignition

Figure 7: High speed imaging. 540 Vdc arc, 30 A, atmospheric pressure, copper cables.

4.2. Erosion of the electrodes

The figure 8 depicts the typical scheme of the erosion of the electrodes. At the beginning (figure 8a), the arc is more or less well confined between the two cables. Then it randomly moves along the stripped part of the cables (about 10 mm long), while also ejecting a lot of droplets of melted metal (figure 8b). Occasionally, the arc does not stay confined and extends its length (figure 8c). These sudden extensions correspond to the brief voltage peaks as we can see in figure 6. Finally, the erosion of the electrodes ends up with the total cut of the cables (figure 8d). In this final stage, the arc is more stable. We no longer see big and random arc extensions and the arc behaviour seems to be driven only by the cathode and anode jets directed in a single direction.

The table 4 shows the ablated mass in mg for every configuration. Let us first compare AC and DC. For both copper and aluminium cables, DC always causes more degradation than AC. It is obviously due to the plasma-off phase in AC, which decreases the effective lifetime of the arc. We also identified the difference between AC and DC on the length of ablated cable, as shown in figure 9. We can see that in DC the erosion length is greater for the cathode than for the anode. This is likely due to the difference of voltage drop between the anode and the cathode. Voltage drop at the cathode is generally two times greater than at the anode.

Comparison between copper and aluminium shows a clear trend. Ablated mass of copper cables is 371 mg on average and 306 mg for aluminium cables. A lower electrode voltage drop for copper than for aluminium electrodes ($18\,V$ and $19\,V$ respectively), involves less energy (difference of 5%, considering the same current) available for copper cable degradation. On the other hand, less energy is needed to ablate one gram of copper and this is why the ablated mass of copper is higher than for aluminium. Indeed, the energy per unit mass for melting the material is 40% lower for copper ($672\,J.\,g^{-1}$) than for aluminium ($1067\,J.\,g^{-1}$). These energies, as well as the densities and the amount of substance for copper and aluminium, are shown in table 3. Although aluminium has a

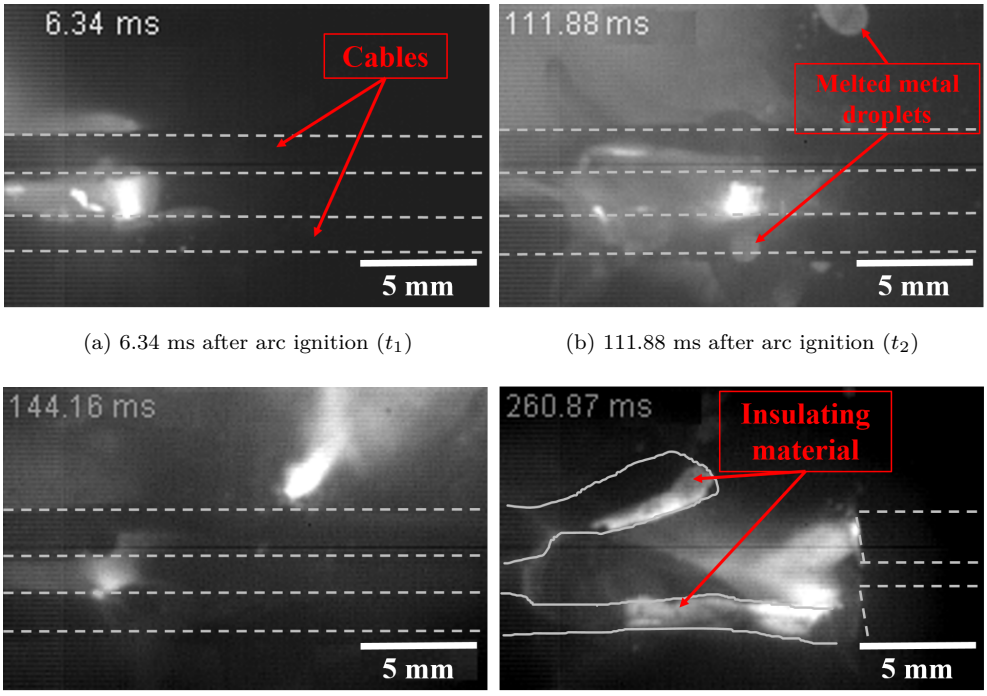

(a) 6.34 ms after arc ignition (t_1)

(b) 111.88 ms after arc ignition (t_2)

(c) 144.16 ms after arc ignition (t_3)

(d) 260.87 ms after arc ignition (t_4)

Figure 8: Typical evolution of the arc fault. Cables are connected to the power supply at the right.

	Atmospheric pressure		Low pressure (95 mbar)	
	AC	DC	AC	DC
Copper cables	-	404 ± 139	331 ± 74	377 ± 98
Aluminium cables	223 ± 17	329 ± 20	265 ± 9	325 ± 27

Table 4: Ablated mass in mg for copper and aluminium cables after arcing.

higher energy per unit mass for melting and therefore less mass is ablated, its lower density involves a higher ablated volume than for copper. The result is a higher erosion speed with aluminium cables. We define the erosion speed as $v_{erosion} = m_{melt} \times (t_{arc} \times \lambda)^{-1}$ where λ is the linear density of the cable material which is obtained experimentally. We found that the erosion speed is about $4.5\,cm.\,s^{-1}$ for copper cables and $6\,cm.\,s^{-1}$ for aluminium cables.

As described in section 3.2.1, the power balance allows us to obtain the vaporised mass of the electrodes. The results in the table 5 represent the fraction of vaporised material with respect to the total ablated mass of metal. The number shown below, in parenthesis, is the corresponding vaporised mass in mg. Let us remind that these results are obtained with some assumptions

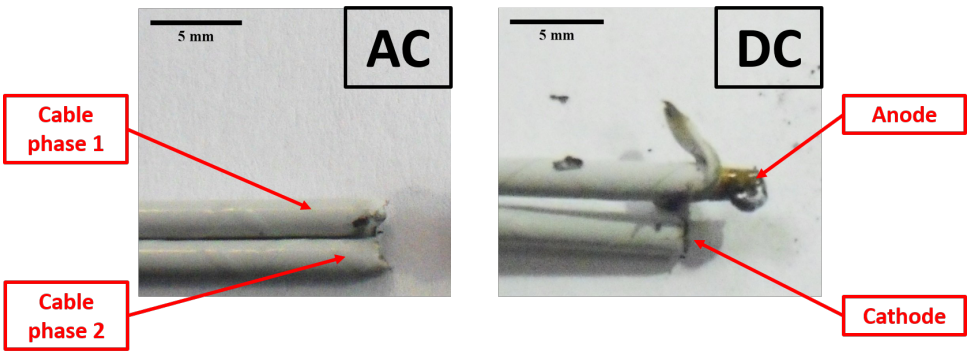

Figure 9: Typical AC and DC erosion after arc fault tests.

	Atmospheric pressure		Low pressure (95 mbar)	
	AC	DC	AC	DC
Copper cables	-	13.71 ± 1.43% (53.10 mg)	4.44 ± 0.95% (13.29 mg)	6.82 ± 1.58% (21.57 mg)
Aluminium cables	8.40 ± 1.40% (14.51 mg)	10.96 ± 1.58% (28.25 mg)	1.93 ± 0.69% (3.81 mg)	1.59 ± 1.44% (3.66 mg)

Table 5: Percentage of electrode vaporisation with respect to the ablated mass.

that allow to figure out the upper boundary values of the vaporised mass. Higher percentages of electrode vaporisation are found for copper cables because of a lower vaporisation energy (see table 3). The vaporised mass is $29.3\,mg$ on average for copper and only $11.9\,mg$ for aluminium. However, converting these masses into amount of substance, we found quite similar values: $4.6.\,10^{-4}\,mol$ for copper and $4.4.\,10^{-4}\,mol$ for aluminium. Regarding the wave form, we observe that the electrode vaporisation is generally higher in DC than in AC. This may be due to an efficient ablation and heating of the electrodes in DC, without the plasma-off phase in AC. We do not observe this trend for aluminium cables at low pressure but the electrode vaporisation is so low that the change from AC to DC may not involve a significant increase. We also see a strong difference between the two pressures. At low pressure, the erosion is much less efficient. It is mainly due to lower electrode voltage drop for both aluminium and copper (about 12 V).

Table 6 shows the specific erosion in $mg.\,C^{-1}$. It is calculated by dividing the ablated mass by the total charge dissipated in the arc ($Q = \int i(t)\,dt$). This quantity depends on the material and the pressure. It is higher for copper and higher at atmospheric pressure for the same reasons as seen above. We can see, taking into account the standard deviation, that it is not correlated with the wave form of the current.

	Atmospheric pressure		Low pressure (95 mbar)	
	AC	DC	AC	DC
Copper cables	-	9.80 ± 2.81	8.97 ± 2.05	8.63 ± 2.24
Aluminium cables	8.32 ± 0.56	7.61 ± 0.52	7.23 ± 0.26	7.47 ± 0.62

Table 6: Specific erosion in mg/C.

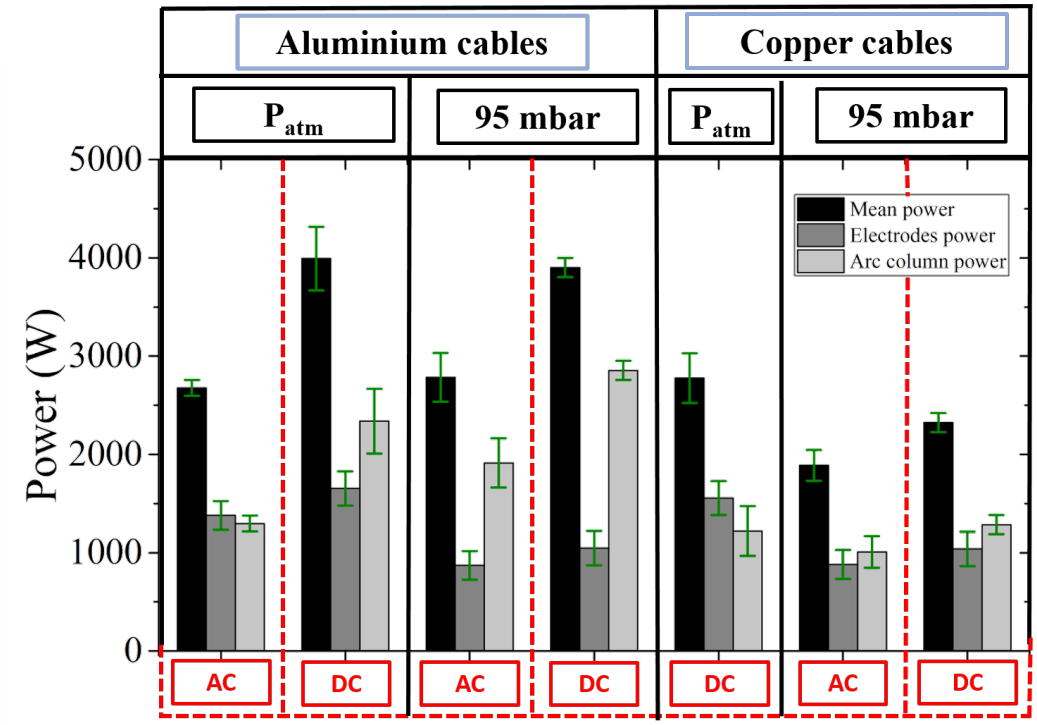

Figure 10: Power balance of the arc faults in AC and DC, for copper and aluminium cables, at atmospheric pressure and low pressure.

4.3. Power balance

The distribution between power in the arc column and transferred to the electrodes is discussed first. The radiated power is discussed after.

Results of the power balance is shown in figure 10. We represent for all configurations, the power transferred to the electrodes in dark grey, the power deposited in the arc column in light grey and the total power in black which is the sum of the two first ones. Standard deviation are represented in green. We discuss in the next sections the influence of each parameters on the arc faults.

4.3.1. Effect of wave form

The main goal of this section is to quantify how much the waveform can impact the mean power of the arc and the distribution between power in the arc column and in the electrodes.

Let us first observe the influence of AC and DC waveform on the mean power of the arc represented by the black columns, in figure 10. In every case, the mean power of the arc is higher in DC than in AC. It is an obvious effect of the null current step in AC, which decreases the lifetime of the arc. This observation is much more important for Al cables than for Cu cables. With Al cables, the increase of mean power from AC to DC is 49% at atmospheric pressure and 41% at 95 mbar, while the increase is only 23% for Cu cables at 95 mbar. The re-ignition of the arc after each null current step at half period may explain the difference between the two pressure for Al cables. For every half period, the voltage has to reach higher values at atmospheric pressure than at 95 mbar for the re-ignition of the arc to take place. It results in a longer re-ignition delay at atmospheric pressure, which decreases the effective lifetime of the arc at each half period. This may explain why the increase of power from AC to DC is more pronounced at atmospheric pressure.

The power balance shows that the change from AC to DC increases significantly the power in the arc column, while the power transferred to the electrodes stays quite similar. In AC, the arc does not have the time between each half period to expand and reach longer arc columns length, while in DC, fast imaging shows higher expansion of the arc and thus, higher voltages in DC. The trend is much more visible for Al cables than for Cu cables, and seems to be a consequence of the spatial arc expansion which is more important for Al cables than for Cu cables. The differences between aluminium and copper are discussed below.

4.3.2. Effect of electrode material

For both aluminium and copper cables (having an identical cross section), the very strong erosion of the cables means that the plasma is highly contaminated with either aluminium or copper vapour. It results in a distinguishable arc behaviour, depending on the material conductor of the cable. First and foremost, the mean power of the arc is considerably higher with aluminium cables. The increase from copper to aluminium cables is about 46% in AC and 68% in DC both at 95 mbar, and the increase is 43% for DC at atmospheric pressure. Such an increase with aluminium cables can not be explained only by the electrodes drop voltage, which is slightly higher for aluminium (19 V) than for copper (18 V). The main reason could be the electrical conductivity of the plasma. For a given current density, Ohm's law implies that the electric field strength should be higher when the electrical conductivity decreases ($j = \sigma E$). Therefore, an aluminium-contaminated plasma, because of a lower electrical conductivity, would need a higher voltage than copper-contaminated plasma, to sustain itself, resulting in an increase of the mean power. The power balance also shows that the power of the arc column is on average more important when using aluminium cables than copper cables. This implies higher arc column lengths with aluminium cables, which is in agreement with

the high-speed imaging observations. Higher column lengths involve higher arc voltages, which in return imply higher power.

Besides, with a more effective vaporisation of the electrode with copper cables (see section 4.2), we can assume that the electron density is higher with copper than with aluminium cables. A higher electron density would increase even more the electrical conductivity of the plasma, and therefore it would reduce the arc voltage. Other mechanisms may have an influence on the arc voltage, but the knowledge of the plasma composition would be necessary.

4.3.3. Effect of pressure

The effect of the pressure shows different trends depending on the cable material. If we focus first on copper cables in DC, we see that the mean power is higher at atmospheric pressure than at low pressure, increasing of about 19%. For an identical arc length, the total arc voltage ($U_{arc} = U_{col} + U_{el}$) is lower at 95 mbar than at atmospheric pressure. This behaviour is not found for aluminium cables: either in AC or DC, the mean power is very similar between the two pressures. It seems that, once the erosion of the electrodes is sufficient and the cables have been totally cut, the arc is no longer confined between the two cables, and is free to expand. Thus, the arc reaches longer lengths than at atmospheric pressure, involving a voltage that is finally similar to the atmospheric pressure case. This is what we observe on the figure 11. Both images are taken from the high-speed camera which was set at 26 000 FPS, with an exposure time of 20 μs and an identical aperture of the lens. Left and right images show an arc performed with aluminium cables, the current was set at 80 A in DC and the images correspond to similar arc duration, that is to say about 494 ms after the ignition. The arc on the left image has been realised at atmsopheric pressure, while on the right image the pressure is set to 95 mbar (brightness and contrast have been adjusted). The red arrows indicate roughly the arc length, and show clearly the difference between the pressures. The arc length appears much longer at low pressure, and it therefore compensates for a lower arc voltage it would have, if the arc length was smaller.

Power distribution between arc column and electrodes shows an increase in arc column power at low pressure. For the same reason as described above, lower pressures involve higher arc column lengths.

4.4. Power lost by radiation

Results of the power lost by radiation are shown in table 7. It is also indicated, in parenthesis, the fraction of radiated power with respect to the mean power of the arc. First of all, we observe that the radiated power is quite low in some cases. It is always less than 10% of the mean power, even though these losses are possibly a bit underestimated, because first, the VUV part of the radiation could not be measured and second, there is probably a small portion of the radiation that is absorbed by the metallic vapour.

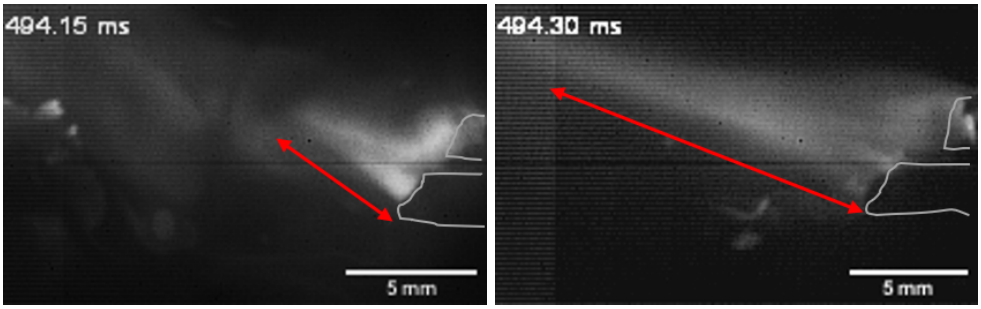

(a) Atmospheric pressure (b) Low pressure

Figure 11: Arc lengths in DC with aluminium cables at 80 A (exposure time : 20 µs). Red arrows indicate estimated arc length.

	Atmospheric pressure		Low pressure (95 mbar)	
	AC	DC	AC	DC
Copper cables	-	158 ± 70 W (5.7%)	24 ± 14 W (1.2%)	43 ± 15 W (1.8%)
Aluminium cables	191 ± 30 W (7.1%)	379 ± 73 W (9.5%)	57 ± 21 W (2.0%)	79 ± 38 W (2.0%)

Table 7: Radiative losses of the arc faults between aluminium and copper cables, in AC and DC, at atmospheric pressure and low pressure. The fraction of radiated power with respect to the mean power of the arc is also indicated in parenthesis.

The part of radiative losses does not change significantly when switching from AC to DC. This part represents about 2% of the mean power of the arc at low pressure for both cable types in AC and in DC. At atmospheric pressure and with Al cables, the part of radiative losses is about 7% in AC and 9.5% in DC. In absolute values, the radiative losses are about twice higher in DC than in AC. As we have seen with the power balance above, the plasma-off phase in AC and the increase of the arc column power in DC are the main causes of the increase of radiative losses that we observe in DC.

A small fraction of metallic vapour which contaminates a plasma in air, is able to change its properties. Especially the radiation emitted by the plasma will be significantly increased with addition of just 1% of metallic vapour [34]. In our case, we found that aluminium has a stronger effect on the radiative losses than copper. They increase much more than the mean power of the arc when replacing copper by aluminum. Despite the possibly lower electron density and the lower electrode vaporisation with aluminium cables, the power in the arc column with aluminium vapour is higher than with copper vapour. In addition, the higher radiative losses with aluminium may be due to the atomic properties, namely lower excitation and ionisation energies for aluminium than

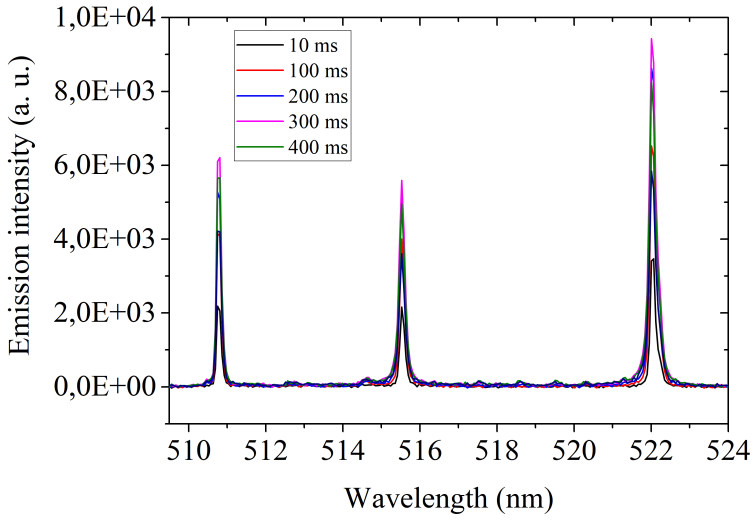

Figure 12: Emission spectra between 510 and 524 nm in the case of a 10 A arc fault between aluminium cables at atmospheric pressure. The spectra are taken at different arc times, and the integration time is 10 ms.

for copper.

Finally, there are much more radiative losses at atmospheric pressure. It is mainly due to a lower density of all the emissive species in the plasma. In addition, we found a lower electrode vaporisation for low pressure arcs (see section 4.2), which involves a lower quantity of the metallic species, the most emissive ones in the plasma.

4.5. Arc fault temperature

For OES measurements, the presence of self-reversed atomic lines of Cu I can be seen for current levels above 25 A. We therefore realised the Boltzmann plot method for 10 A current level only, and assuming that the plasma is in Local Thermodynamic Equilibrium (LTE). At this current intensity, we did not find any self-reversed atomic lines. An example of the spectra used for the Boltzmann plot method can be found in figure 12. This spectra is obtained with an arc ignited between aluminium cables at 10 A and at atmospheric pressure. The three emission lines of Cu I are well separated, and they provide a sufficient energy range (according to [25]) to apply the Boltzmann plot method with a good accuracy. It should be noted that in this example, the temporal evolution of the emission intensities is not relevant. Indeed, the peak intensities may vary randomly during an arc, and there is no trend we can deduce from the temporal evolution of the emission lines (this is in agreement with the results of the high speed imaging with filters).

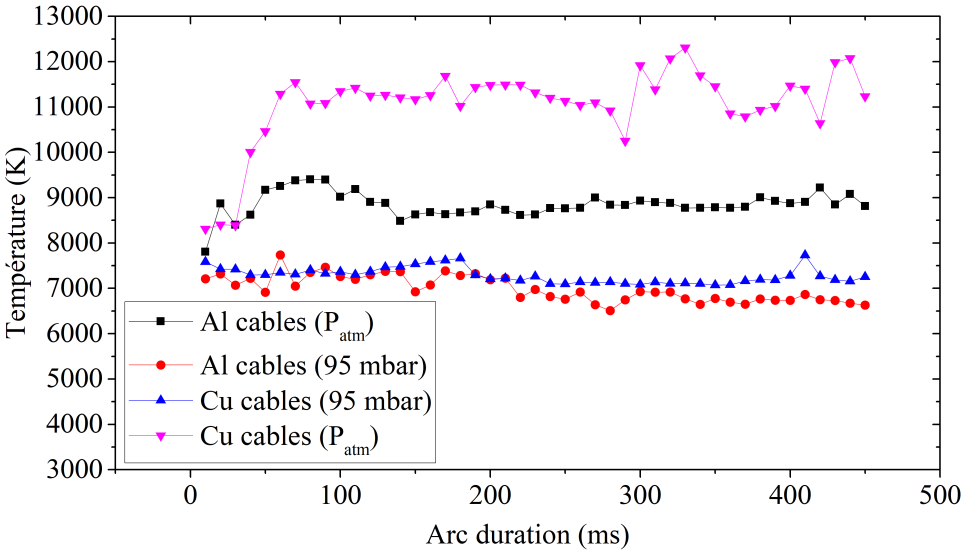

Figure 13: Overall plasma temperature evolution obtained using the Boltzmann plot method.

The literature shows that the dependence of the plasma temperature on the arc current is not very important between 10 A and 100 A [33]. We therefore assume that the results for arcs at 10 A are quite similar at 80 A. Although the arcs are very erratic, the trend on the temperature is reproducible. Figure 13 shows the typical temporal evolution of the overall temperature for an arc fault in four configurations: Al and Cu cables at atmospheric pressure and 95 mbar. As previously explained in section 2.2, the obtained temperatures represent a spatially-average temperature of the plasma (the overall plasma temperature), and the plasma is assumed to be in LTE. It appears from figure 13, that the temperatures are quite constant during the whole arc duration. Although the arc length increases as the electrodes are being ablated by the arc, the temperatures do not show a strong temporal dependence. However, noticeable differences occur between Cu and Al cables at atmospheric pressure only. Despite of a lower arc voltage with a higher thermal conductivity for Cu, we observe that Cu contaminated plasma has a higher temperature (~ 10500 K) than Al plasma (~ 8500 K). The higher radiative losses obtained previously for Al plasma in the power balance, may explain the lower temperature. We also observe a significant decrease in temperature at low pressure for both cables (~ 7000 K).

5. Summary

We studied arc fault between aeronautic cables for the assessment of a power balance. The tests took place in a chamber at atmospheric pressure and at 95 mbar, with Al and Cu cables. Since the

new trend in the aeronautic industry might lead to the use of DC architectures instead of traditional AC, we tested the cables with both AC and DC currents. It appears that the change from AC to DC increases the mean power of the arc. The plasma-off phase in AC is obviously the main reason, but we also notice lower voltage in AC than in DC. This behaviour is more pronounced with Al cables than with Cu cables. We quantify the increase of the mean power from AC to DC of 23% for Cu cables and 45% for Al cables. This increase of mean power in DC is mainly lost by conduction, convection and radiation, since arc column lengths, and thus the power in the arc column are higher in DC than in AC. The plasma contaminated with metallic vapour, shows important differences between Al and Cu, on the mean power, the arc length, the radiative losses and the temperature. Higher radiative losses for Al than for Cu, make the Al plasma cooler compared to Cu plasma. Besides, the mean power is significantly lower for Cu than for Al plasma.

References

[1] B. G. Moffat, E. Abraham, M. P. Y. Desmulliez, D. Koltsov and A. Richardson, "Failure mechanisms of legacy aircraft wiring and interconnects", *IEEE Transactions on Dielectrics and Electrical Insulation*, vol. 15, no. 3, pp. 808-822, June 2008.

[2] F. Dricot et H. J. Reher, "Survey of arc tracking on aerospace cables and wires", *IEEE Trans. Dielectr. Electr. Insul.*, vol. 1, no 5, p. 896–903, 1994.

[3] J. Hanson and D. Koenig, "Fault arcs effects in cable bundles for space applications in vacuum", *IEEE Transactions on Dielectrics and Electrical Insulation*, vol. 4, no. 4, pp. 394-399, Aug. 1997.

[4] T. J. Stueber, D. McCall and A. Hammoud, "Comparison of arc tracking tests in various aerospace environments", 1996 *IEEE International Symposium on Electrical Insulation*, Montreal, Quebec, Canada, pp. 349-352 vol.1.

[5] F. R. Frontzek, D. Koenig, M. D. Judd, and H. J. Reher "Phenomena of fault-arc propagation on cables and wires for space applications in vacuum and oxygen-enriched atmosphere and air", Proc. SPIE 2259, *XVI International Symposium on Discharges and Electrical Insulation in Vacuum*, (1 May 1994).

[6] I. Christou, A. Nelms, I. Cotton and M. Husband, "Choice of optimal voltage for more electric aircraft wiring systems", *IET Electrical Systems in Transportation*, vol. 1, no. 1, pp. 24-30, March 2011.

[7] A. Lücken, J. Brombach and D. Schulz, "Design and protection of a high voltage DC onboard grid with integrated fuel cell system on more electric aircraft", *Electrical Systems for Aircraft, Railway and Ship Propulsion*, Bologna, 2010, pp. 1-6.

[8] D. Izquierdo, R. Azcona, F. J. L. d. Cerro, C. Fernández and B. Delicado, "Electrical power distribution system (HV270DC), for application in more electric aircraft," 2010 *Twenty-Fifth Annual IEEE Applied Power Electronics Conference and Exposition (APEC)*, Palm Springs, CA, 2010, pp. 1300-1305.

[9] P. Teste, T. Leblanc, R. Andlauer and J-P. Chabrerie, "Copper cathode erosion by an electric arc—the causes of the variations of the erosion rate with the electrode gap", 2001 *Plasma Sources Sci. Technol.* **10** 10

[10] L. Chemartin, P. Lalande, E. Montreuil, C. Delalondre, B.G. Chéron, F. Lago, "Three dimensional simulation of a DC free burning arc. Application to lightning physics", *Atmospheric Research*, Volume 91, Issue 2, p. 371-380

[11] Y. Wu, M. Li, M. Rong, F. Yang, A. B Murphy, Y. Wu and D. Yuan , "Experimental and theoretical study of internal fault arc in a closed container", 2014 *J. Phys. D: Appl. Phys.* **47** 505204

[12] M. Eblen and T. Short, "Low-voltage arc sustainability", 2017 *IEEE IAS Electrical Safety Workshop (ESW)*, Reno, NV, 2017, pp. 1-13

[13] Y. Wu, Y. Cui, M. Rong, A. B Murphy, F. Yang, H. Sun, C. Niu and S. Fan, "Visualization and mechanisms of splashing erosion of electrodes in a DC air arc*",* 2017 *J. Phys. D: Appl. Phys.* **50** 47LT01

[14] M. Li, Y. Wu, P. Gong, L. Li, H. Xu and F. Yang, "Experimental investigation of thermal transfer coefficient by a simplified energy balance of fault arc in a closed air vessel", 2020 *Plasma Sci. Technol.* **22** 024001

[15] T. André, F. Valensi, P. Teulet, Y. Cressault, T. Zink and R. Caussé , "Arc tracking energy balance for copper and aluminum aeronautic cables", 2017 *J. Phys.: Conf. Ser.* **825** 012001

[16] H. El Bayda, F. Valensi, M. Masquere and A. Gleizes, "Energy losses from an arc tracking in aeronautic cables in DC circuits", *IEEE Transactions on Dielectrics and Electrical Insulation*, vol. 20, no. 1, pp. 19-27, February 2013.

[17] F Valensi, S. Pellerin, A. Boutaghane, K. Dzierzega, S. Zielinska, N. Pellerin and F. Briand, "Plasma diagnostics in gas metal arc welding by optical emission spectroscopy", 2010 *J. Phys. D: Appl. Phys.* **43** 434002

[18] F. Wang, Y. Cressault, P. Teulet, F. Valensi, H. Li, K. Yang and F. Yu, "Spectroscopic investigation of partial LTE assumption and plasma temperature field in pulsed MAG arcs", 2018 *J. Phys. D: Appl. Phys.* **51** 255203

[19] T. André, "Étude des mécanismes d'entretien et de propagation d'un arc électrique de court-circuit entre câbles endommagés dans les réseaux électriques d'aéronefs", 2017, Ph.D. Thesis, University Paul Sabatier Toulouse 3

[20] N. K. Joshi, S. N. Sahasrabudhe, K. P. Sreekumar and N. Venkatramani, "Variation of axial temperature in thermal plasma jets", 1997 *Meas. Sci. Technol.* **8** 1146

[21] R. Kozakov, M. Kettlitz, K-D. Weltmann, A. Steffens and C. M. Franck, "Temperature profiles of an ablation controlled arc in PTFE: I. Spectroscopic measurements", 2007 *J. Phys. D: Appl. Phys.* **40** 2499

[22] X. Hao and G. Song, "Spectral Analysis of the Plasma in Low-Power Laser/Arc Hybrid Welding of Magnesium Alloy", 2008 *IEEE Transactions on Plasma Science*, vol. 37, no. 1, pp. 76-82

[23] J. Zalach and St. Franke, "Iterative Boltzmann plot method for temperature and pressure determination in a xenon high pressure discharge lamp", 2013 Journal of Applied Physics **113**, 043303

[24] R. Sousa Martins, C. Zaepffel, L. Chemartin, P. Lalande and A. Soufiani, "Characterization of a high current pulsed arc using optical emission spectroscopy", 2016 *J. Phys. D: Appl. Phys.* **49** 415205

[25] Kramida, A., Ralchenko, Yu., Reader, J., and NIST ASD Team (2019). NIST Atomic Spectra Database (ver. 5.7.1), [Online]. Available: https://physics.nist.gov/asd [2020, March 30]. National Institute of Standards and Technology, Gaithersburg, MD. DOI: https://doi.org/10.18434/T4W30F

[26] F. Valensi, P. Ratovoson, M. Razafinimanana and A. Gleizes, "Anode energy transfer in a transient arc", 2017 *J. Phys.: Conf. Ser.* **825** 012018

[27] D. Godin, J. Y. Trépanier, M. Reggio, X. D. Zhang and R. Camarero, "Modelling and simulation of nozzle ablation in high-voltage circuit-breakers", 2000 *J. Phys. D: Appl. Phys.* **33** 2583

[28] Chase M W 1998, NIST-JANAF Thermochemical Tables. Washington, DC: New York: American Chemical Society ; American Institute of Physics for the National Institute of Standards and Technology

[29] P. Teulet, T. Billoux, Y. Cressault, M. Masquère, A. Gleizes, I. Revel, B. Lepetit, G. Peres, "Energy balance and assessment of the pressure build-up around a bolt fastener due to sparking during a lightning impact", 2017 Eur. Phys. J. Appl. Phys. **77** (2) 20801

[30] F. Lago, 2004, Ph.D. Thesis, University Paul Sabatier Toulouse 3

[31] F. Lago, J.J. Gonzalez, P. Freton, A. Gleizes, "A numerical modelling of an electric arc and its interaction with the anode: Part I. The two dimensional model", 2004 *J. Phys. D: Appl. Phys.* **37** 883

[32] R. Holm, "The Vaporization of the Cathode in the Electric Arc", 1949 *Journal of Applied Physics* **20** 715

[33] J. J. Lowke, "Simple theory of free-burning arcs", 1979 *J. Phys. D: Appl. Phys.* **12** 1873

[34] Y. Cressault, R. Hannachi, P. Teulet, A. Gleizes, J-P. Gonnet and J-Y. Battandier, "Influence of metallic vapours on the properties of air thermal plasmas", 2008 *Plasma Sources Sci. Technol.* **17** 035016